# Surface Reactivity of a Carbonaceous Cathode in a Lithium Triflate/Ether Electrolyte-Based Li−O$_2$ Cell

Marco Carboni,[†] Sergio Brutti,[‡] and Andrea G. Marrani[*,†]

[†]Department of Chemistry, Sapienza University of Rome, P.le Aldo Moro 5, Rome 00185, Italy

[‡]Department of Science, University of Basilicata, V.le Ateneo Lucano 10, Potenza 85100, Italy

S *Supporting Information*

ABSTRACT: Li−O$_2$ batteries are currently one of the most advanced and challenging electrochemical systems with the potential to largely overcome the performances of any existing technology for energy storage and conversion. However, these optimistic expectations are frustrated by the still inadequate understanding of the fundamentals of the electrochemical/chemical reactions occurring at the cathode side, as well as within the electrolyte and at the three-phase interface. In this work, we illustrate the evolution of the morphology and composition of a carbonaceous cathode in the first discharge/charge in a Li−O$_2$ cell with an ether-based electrolyte by X-ray photoemission spectroscopy, Fourier transform infrared spectroscopy, and transmission electron microscopy. Experiments have been carried out ex situ on electrodes recuperated from electrochemical cells stopped at various stages of galvanostatic discharge and charge. Apparently, a reversible accumulation and decomposition of organic and inorganic precipitates occurs upon discharge and charge, respectively. These precipitations and decompositions are likely driven by electrochemical and chemical parasitic processes due to the reactivity of the cathode carbonaceous matrix.

KEYWORDS: *Li−O$_2$ battery, cathode surface reactivity, Fourier transform infrared spectroscopy, transmission electron microscopy, X-ray photoelectron spectroscopy*
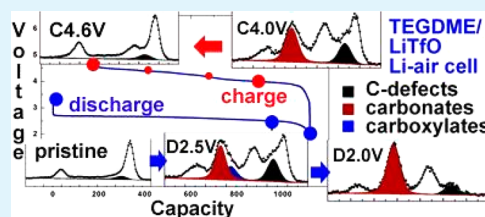
INTRODUCTION

Rechargeable energy storage devices have been widely studied in the last decades.[1,2] In fact, their performances are continuously improved, because electronic devices (mobile phones, tablets, laptop computers, smartphones) require batteries with growing power and energy densities.[3] In this field, Li-ion batteries are a case-study success story due to their unmatched properties: high reversibility, high voltage, high energy density, low self-discharge, reliability, and calendar life.[4,5] Li-ion devices are probably, in this debut of the XXI century, the most popular energy storage systems worldwide. Despite that, commercial Li-ion batteries are apparently not able to provide an adequate power supply to match the need of more challenging applications, like electric vehicles.[6] This evidence is pushing the R&D worldwide efforts toward the investigation of innovative electrochemical systems with drastically improved theoretical performances.

Li−O$_2$ cells are currently one of the most advanced and challenging innovative electrochemical system, with the potential to largely overcome the performances of any competing technology for energy storage and conversion.[7] In fact, the high theoretical energy density, reduced costs, and the ability to take oxygen directly from the environment make, in principle, this new type of device suitable to fulfill all of the severe requirements necessary to successfully power electric vehicles.[8,9] However, these optimistic expectations are currently frustrated by the still inadequate understanding of the fundamentals of the electrochemical/chemical reactions occurring in this apparently simple device.[10] In fact, although many papers are published monthly with outstanding improvements in the reported performances of Li−O$_2$ cells, the mechanism of O$_2$ reduction and evolution (oxygen reduction reaction, ORR, and oxygen evolution reaction, OER, respectively) at the three-phase interface (O$_2$, liquid electrolyte, cathode surface) on the cathode side of the cell has not been so far fully elucidated and understood.

The general consensus[9,10] suggests that a Li−O$_2$ cell operates by reversibly forming and decomposing Li$_2$O$_2$ particles precipitated on the pores of a gas-permeable cathode, through the electrochemical reduction/oxidation of gaseous oxygen molecules. However, many authors demonstrated a much more complex picture where other chemical species (e.g., LiO$_2$, Li$_2$O, Li$_2$CO$_3$) are formed and decomposed in discharge and charge, respectively. Apparently, the occurrence of these parallel reactive paths is modulated by the choice of electrolyte components, as well as the nature of the porous cathode surface. In particular, the coupling of ether-based solvents (e.g., tetraethylene glycol dimethyl ether, TEGDME), inorganic fluorine-free lithium salts (e.g., lithium triflate, LiTfO), and carbonaceous catalysis allows one to achieve outstanding performances in terms of capacity as well as cycling reversibility.[10]

This competition between the reversible Li$_2$O$_2$ formation/decomposition and other chemical and electrochemical

© 2015 American Chemical Society
21751
DOI: 10.1021/acsami.5b05202
ACS Appl. Mater. Interfaces 2015, 7, 21751−21762

processes occurring on the electrodes leads to a surprisingly large difference between the chemical (O_2 consumption/production yield between discharge and charge) and the electrochemical (Coulombic efficiency) reversibility of Li−O_2 cells.[11] Moreover, the formation of insoluble reaction byproducts that accumulates upon cycling within the pores of the cathode is responsible for the fading of the performances and the death of the device.[12]

In this work, we illustrate the evolution of the morphology and composition of a carbonaceous cathode in the first discharge/charge in a Li−O_2 cell with an ether-based electrolyte by X-ray photoemission spectroscopy (XPS), Fourier transform infrared spectroscopy (FTIR), and transmission electron microscopy (TEM). Experiments have been carried out ex situ on electrodes recuperated from electrochemical cells stopped at various stages of galvanostatic discharge and charge. The goal is to describe the occurrence of an extended chemical degradation of the carbonaceous catalyst and modification of the cathode surface upon reduction/oxidation.

■ EXPERIMENTAL SECTION

Li−O_2 cells have been assembled by using a MTI Corp. stainless steel lithium−air test cell. The cell assembly has been made by coupling a metallic lithium foil as anode, a glass-fiber separator (Whatman) impregnated with a nonaqueous electrolyte, and a commercial porous carbon foil (MTI Corp., 15 mm in diameter) as cathode. The cathode foil is constituted by a mixture of SuperP carbon and a Teflon binder dispersed on an inert carbonaceous gas diffusion layer (38:62 w/w ratio SuperP carbon/binder). The electrolyte is a 1 molal solution of lithium triflate (LiCF$_3$SO$_3$) in tetraethylene glycol dimethyl ether (TEGDME, Sigma-Aldrich, moisture controlled grade). Cells and electrolyte solutions have been prepared in a Iteco Engineering argon-filled glovebox with moisture concentration below 0.1 ppm. The lithium triflate salt and porous cathodes have been dried at 110 °C overnight under vacuum before use. The TEGDME solvent has been used after drying/storage on regenerated 3 Å molecular sieves (Sigma-Aldrich) and lithium chips for at least 15 days in a glovebox. The Li−O_2 cells have been filled with an high-purity atmosphere of O_2 (5.0 purity, spilled from a high-pressure cylinder through a stainless steel gas lines, preliminarily evacuated, equipped with a molecular sieve-filled moisture trap). A static final pressure of 2.2 bar has been set for all tests: the final partial pressure of molecular oxygen in the dead volume (approximately 3 cm^3) above the porous electrode within the cell is 1.2 bar.

Electrochemical tests have been carried out by means of a MTI Corp. battery cycler in galvanostatic conditions, adopting a constant current of 0.1 mA cm^{-2}. The measured capacity has been normalized to specific values for only the weight of SuperP carbon catalyst.

After the electrochemical tests, the carbonaceous cathodes have been recuperated from the cell, washed in TEGDME and tetrahydrofuran (THF) three times to remove the electrolyte residues, and dried under vacuum at room temperature. Handling of all materials, samples (pristine and recuperated from test cells), and unsealed cells has been carried out in a Iteco Engineering argon-filled glovebox, with moisture concentration below 0.1 ppm.

Carbonaceous cathodes, as well as the benchmark materials, have been characterized by X-ray photoemission spectroscopy (XPS), Fourier transform infrared spectroscopy (FTIR), and transmission electron microscopy (TEM).

XPS measurements have been carried out using a modified Omicron NanoTechnology MXPS system equipped with a mono-chromatic X-ray source (Omicron XM-1000) and an Omicron EA-127 energy analyzer. The exciting radiation was Al Kα ($h\nu$ = 1486.7 eV), generated operating the anode at 14−15 kV and 10−20 mA. All of the photoionization regions have been acquired using an analyzer pass energy of 20 eV, except for the survey scan, which has been taken at 50

eV pass energy. Take-off angles of 11° with respect to the sample surface normal have been adopted. The measurements have been performed at room temperature, and the base pressure in the analyzer chamber was about 2 × 10^{-9} mbar during the spectra detection. The C 1s binding energy (BE) of the amorphous carbonaceous (graphite-like) component at 284.30 eV has been used as an internal standard reference for the BE scale (accuracy of ±0.05 eV). Samples have been transferred into the spectrometer through an argon-filled glovebag directly connected to the fast-entry lock chamber of the instrument without contact with air, to avoid possible moisture/CO_2 contaminations. The experimental spectra have been theoretically reconstructed by fitting the secondary electrons' background to a Shirley function and the elastic peaks to pseudo-Voigt functions described by a common set of parameters (position, fwhm, Gaussian−Lorentzian ratio) free to vary within narrow limits. The Gaussian−Lorentzian ratio varied between 0.7 and 0.9. XPS atomic ratios (±10% associated error) between relevant core lines have been estimated from experimentally determined area ratios corrected for the corresponding Scofield cross sections[13] and for a square root dependence of the photoelectrons kinetic energies. No sign of sample degradation upon extended acquisition times under the X-rays has been observed.

The FTIR spectra have been acquired by a Jasco FTIR-300 apparatus. All spectra have been recorded in the wavenumber range between 2000 and 400 cm^{-1} at room temperature in transmission mode. The samples, as fine powder, have been mixed in the Ar-filled glovebox with CsI in a ratio of 1:100 mg (powder to CsI, respectively) and then pressed in pellets by a Pike die set and hand-press.
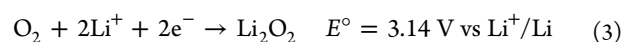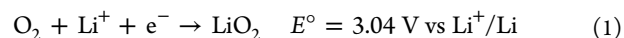
TEM micrographs have been recorded by using a FEI G2 20 HR-TEM instrument equipped with a LaB$_6$ electron beam source and two 2D flat cameras (low resolution and high resolution) at 200 kV e-beam acceleration. Samples have been suspended in THF in sealed vials by ultrasonic treatment (5 cycles of 15 min of ultrasonic treatment followed by 45 min of rest to cool the sample and thus avoid thermal heating), and dispersed on copper holey carbon film grids for observation.
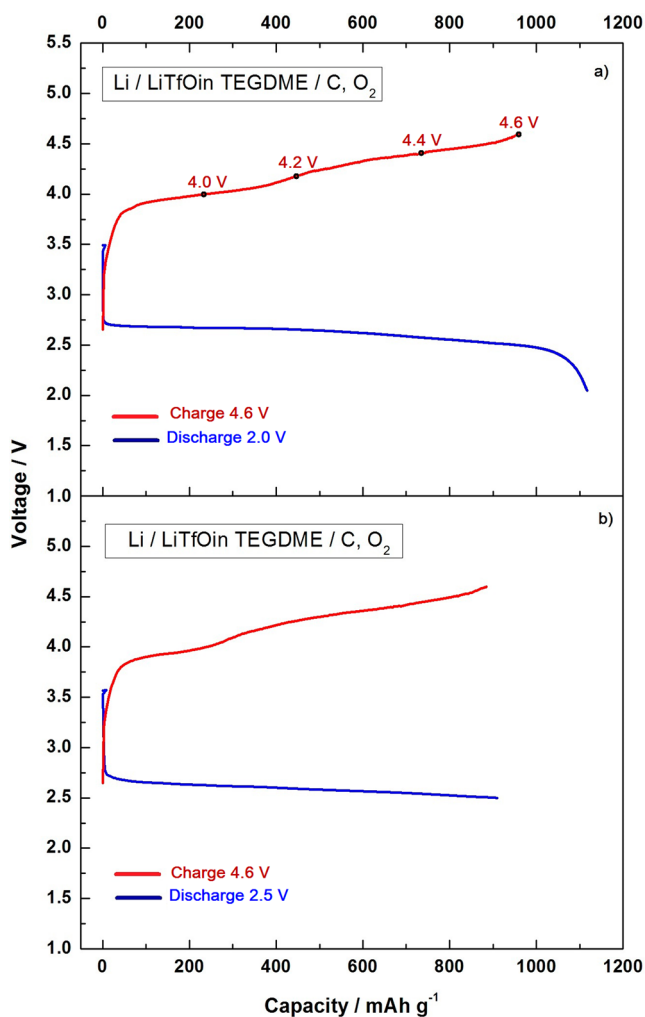
■ RESULTS AND DISCUSSION

Electrochemical Tests. Cells have been partially and/or fully cycled in galvanostatic tests. Examples of the typically measured voltage profiles are shown in Figure 1 for two cells fully cycled between 2.0 and 4.6 V, and 2.5 and 4.6 V. In this Article, our goal is to highlight new insights and elucidate the evolution of the surface chemistry in the first discharge/charge cycle of carbonaceous electrodes in nonaqueous Li−O_2 cells with an ether-based electrolyte.
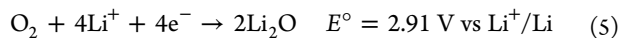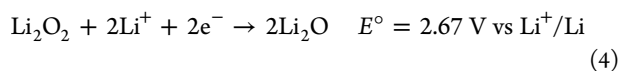
To this aim, the demonstration of outstanding cell performances is beyond the scope of this Article. Nevertheless, the analyses of the properties of the studied cathode material and electrolyte in galvanostatic tests in various cycling conditions are summarized in Table 1, together with the sample coding used throughout the entire text. All of the electrode materials recuperated from the cells, as well as the pristine one, have been submitted to a multiple-technique investigation protocol (XPS, FTIR, and TEM).

Upon discharge, the voltage profiles show the expected stable plateau at about 2.7−2.5 V.[14] This discharge plateau voltage range is below the thermodynamically estimated potential for the expected oxygen reactions upon reduction (see eqs 1−5),[14] thus suggesting the occurrence of moderate overvoltages.

$$O_2 + Li^+ + e^- \rightarrow LiO_2 \quad E° = 3.04 \text{ V vs } Li^+/Li \quad (1)$$

$$LiO_2 + Li^+ + e^- \rightarrow Li_2O_2 \quad E° = 3.25 \text{ V vs } Li^+/Li \quad (2)$$

$$O_2 + 2Li^+ + 2e^- \rightarrow Li_2O_2 \quad E° = 3.14 \text{ V vs } Li^+/Li \quad (3)$$

Figure 1. Galvanostatic cycles between (a) 2.0 and 4.6 V and (b) 2.5 and 4.6 V (cathodic and anodic cutoff voltages for partially discharged and charged cells are shown in (a)).

$$Li_2O_2 + 2Li^+ + 2e^- \rightarrow 2Li_2O \quad E^\circ = 2.67 \text{ V vs } Li^+/Li$$
$$(4)$$

$$O_2 + 4Li^+ + 4e^- \rightarrow 2Li_2O \quad E^\circ = 2.91 \text{ V vs } Li^+/Li \quad (5)$$

These latter are likely due to polarization and surface thermodynamics effects.[15] As a consequence, a clear electrochemical discrimination of the various processes is impossible.

At the end of discharge, the investigated cells are apparently able to incorporate one-half of the available molecular oxygen. With ~0.15 mmol being the total estimated available gaseous

oxygen in the dead volume of the cell, the electrochemical discharge process yields (i.e., the ratio between the measured specific capacity in reduction and the available oxygen moles multiplied by the number of exchanged electrons, 4) are 38% and 47% for electrodes discharged down to 2.5 and 2.0 V, respectively.

Turning to charge processes, as expected, upon oxidation the cells supply an increasing total capacity with the increase of the anodic voltage cutoff, reaching a final Coulombic efficiency of $93.2 \pm 7.5\%$ for the cell fully cycled between 2.0 and 4.6 V. The cell cycled between 2.5 and 4.6 V shows slightly smaller specific capacities and a Coulombic efficiency approaching $97.3 \pm 4.1\%$. This evidence is in agreement with the general consensus about the superior electrochemical reversibility of the Li_2O_2 formation/decomposition reactions that may overlap with the redox reactivity of the Li_2O phase.[12] In fact, the ratio between the formation of Li_2O_2 and Li_2O is expected to decrease by shifting downward the cathodic voltage cutoff.[14]

It is interesting to observe that the voltage profiles in charge of the cells discharged to 2.5 and 2.0 V are different. In particular, the cell discharged to 2.5 V shows an extended low voltage plateau in charge at 3.6–3.8 V followed by a second high voltage stable plateau at 4.4–4.5 V. On the contrary, the cell discharged to 2.0 V gives a more sloping and featureless charge voltage profile. This behavior is expected in ether-based electrolytes where the average plateau potential (U_{chg}) has been already reported to increase upon charge.[11]

In the literature, the complicated dependence of U_{chg} on the charge capacity has been related to a number of possible concurrent factors, for example, the nature of the porous cathode material, the loading of catalyst/carbon, the extent of discharge, the nature of the ether-solvent, etc.[14] However, a clear explanation for this phenomenon is still missing, and different competing hypotheses have been proposed to tackle this controversial point. McCloskey et al.[11] suggest that the potential rise of U_{chg} arises from the deposition of carbonate/carboxylates at the Li_2O_2–electrolyte interface due to electrochemical decomposition of the electrolyte during the charging process. On the other hand, Shao-Horn et al.[16] argue that the different observed plateaus and slopes upon charge may be due to different surface reactions. This picture has been recently supported by the in situ Raman investigation of the Li–O_2 cell discharge products that suggests the presence of thick layers of lithium superoxide on the surface of the Li_2O_2 particles.[17]

Transmission Electron Microscopy. The evolution of the morphology of the cathode active material is reported in Figure 2, where the TEM micrographs of the various studied samples are shown.

Table 1. Summary of the Studied Samples and Corresponding Performances in Galvanostatic Tests[a]

samples	redox end state	end test cell voltage (V)	discharge capacity (mAh g^{-1})	charge capacity (mAh g^{-1})	Coulombic efficiency (%)
D2.5V	reduction	2.5	766 ± 63		
D2.0V	reduction	2.0	956 ± 64		
C4.0V	oxidation[b]	4.0	943 ± 166	298 ± 52	31.6 ± 9.7
C4.2V	oxidation[b]	4.2	1010 ± 99	435 ± 42	43.0 ± 7.3
C4.4V	oxidation[b]	4.4	1019 ± 90	800 ± 70	78.4 ± 6.8
C4.6V	oxidation[b]	4.6	1043 ± 66	972 ± 62	93.2 ± 7.5
D2.5V−C4.6V	oxidation[c]	4.6	910 ± 75	885 ± 71	97.3 ± 4.1

[a]Coulombic efficiencies have been calculated as the ratio between the discharge and the corresponding charge specific capacity. [b]Cell discharged to 2.0 V. [c]Cell discharged to 2.5 V.
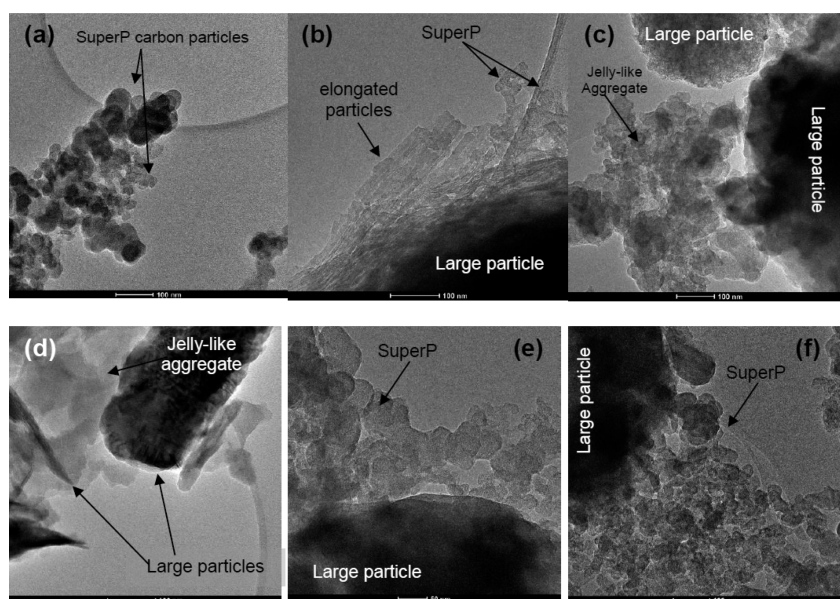
Figure 2. TEM images of the samples: (a) pristine electrode; (b) D2.5V; (c) D2.0V; (d) C4.0V; (e) C4.6V; and (f) D2.5V−C4.6V.
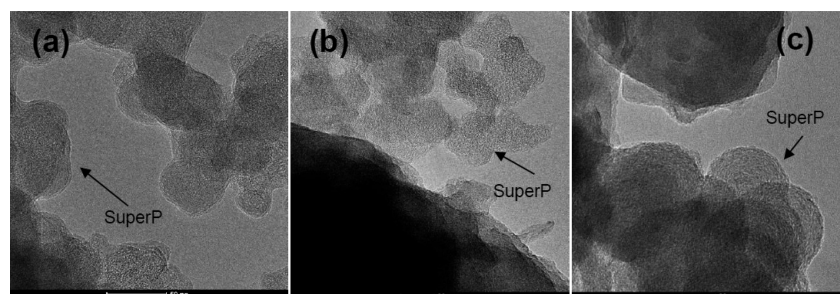
Figure 3. TEM micrographs of the SuperP carbon particles: (a) pristine electrode; (b) C4.6V sample; and (c) D2.5V−C4.6V sample.

The pristine cathode is constituted, as expected, by SuperP carbon round-shaped particles with average diameter of 20−60 nm. Upon discharge other precipitates form around the carbon particles. After discharge to 2.5 V (Figure 2b), a large number of regular thin elongated particles precipitate together in larger irregular aggregates surrounded by almost unaltered SuperP spheres. Within these irregular aggregates, it is possible to highlight the presence of well-crystallized domains as shown in Figure S1a: the FFT of the crystalline domains (see Figure S1b) can be indexed to the hexagonal lattice of Li_2O_2. On the contrary, a clear identification of Li_2O crystallized particles is missing. At deeper discharge (2.0 V, Figure 2c), the morphology evolves due to the accumulation of many large round-shaped particles as large as 500−900 nm. These particles are apparently formed by many smaller particles closely packed between each other, surrounded by an amorphous jelly-like matrix. Some SuperP carbon particles can also be observed embedded within this irregular matrix.[18] Unfortunately, in this complex matrix, a diffraction identification of Li_2O_2 or Li_2O phases is not possible.

Upon charge, further morphological changes occur. The C4.0 V sample, discharged down to 2.0 V and then charged to 4.0 V, still shows a rather large number of homogeneous thin large particles with reduced size (200−400 nm) in comparison to the D2.0V sample: interestingly, these smaller particles show a platelet morphology. Few larger particles can be still observed together with an extended jelly-like matrix constituted by smaller irregular particles mixed with SuperP carbon. At the end of charge at 4.6 V, both cathodes discharged to 2.5 and 2.0 V show similar morphologies. Apparently, few and isolated homogeneous and regular large particles still survive after charge: their morphology is very similar to that observed after discharge to 2.0 V. These particles are likely residual unreacted Li_2O/Li_2O_2 particles, possibly originated from the incomplete back conversion to gaseous oxygen upon charge. Besides these few particles, also SuperP carbon particles are observed. The comparison at high magnification of the shapes of the SuperP carbon particles in the pristine, C4.6V, and D2.5V−C4.6V samples is shown in Figure 3.

After a full cycle in the 2.0−4.6 V range, the originally well-formed round-shaped SuperP carbon particles show irregular surfaces and are apparently reduced in size and closely interconnected in irregular and porous aggregates. On the other hand, after one galvanostatic cycle between 2.5 and 4.6 V, the original SuperP morphology is almost unaltered and thus preserved at the end of the electrochemical test.

In summary, the morphology evolution suggests the occurrence of the expected precipitation and almost complete consumption of Li_2O_2/Li_2O round-shaped particles upon discharge and charge, respectively. These particles are apparently complex aggregates of smaller irregular subparticles with possible elongated shapes with crystalline domains indexed to the Li_2O_2 lattice. Besides this, also other morphological changes occur, in particular, the accumulation

and almost complete removal upon discharge and charge, respectively, of an extended jelly-like matrix that surrounds the SuperP particles. Moreover, the carbon nanoparticles show an unexpected morphological alteration between the pristine and the fully cycled, 2.0 V-discharged sample. This evident alteration of the morphology of the carbon particles is mitigated in the material discharged down to 2.5 V.

FTIR Spectroscopy. In Figure 4 are shown the FTIR spectra of the pristine, discharged, and cycled cathodes. The reference spectra of Li_2O_2 and Li_2O are also shown.

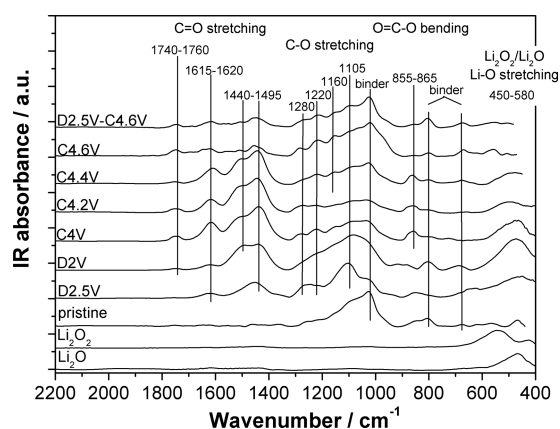**Figure 4.** FTIR spectra of the carbonaceous electrodes.

In the 400−600 cm^{-1} region, where the stretching of Li−O bond is expected, a broad band increases upon discharge and fades upon charge. This band may be due to the overlap of the LiOH, Li_2O_2, and Li_2O vibrational modes.[14] However, the analysis of the spectral ranges between 3000 and 4000 cm^{-1} (not shown) highlights the absence of the sharp absorption bands attributable to LiOH at 3678 or 3574 cm^{-1}, thus excluding the formation of this phase as discharge product. Turning to the other possible phases, although our FTIR spectra are apparently unable to clearly discriminate the formation of Li_2O_2 or Li_2O, the evolution trend of the band below 600 cm^{-1} may suggest the accumulation of lithium oxide upon discharge in the D2V sample and its apparent preferential removal in the first stages of charge (e.g., the comparison between samples D2V, C4V, and C4.2V).

Upon discharge, also other signals increase in the spectral range attributable to the O−C=O bending mode, and C−O and C=O stretching vibrations. These signals are likely due to the possible accumulation of organic esters (C=O asymmetric stretching at 1740−1760 cm^{-1}) and carbonates (C=O asymmetric stretching at 1610−1620 cm^{-1}).[19,20] Also, the clear fingerprint of the inorganic Li_2CO_3 is nicely detected (ν_3 at 1495 and 1440 cm^{-1}, ν_1 at 1090 cm^{-1}, and ν_2 at 860 cm^{-1}),[21,22] whereas the formation of partially oxidized species like lithium oxalate or lithium formate is to be excluded, due to the absence of the expected intense C−O stretching vibrations at 1300−1380 cm^{-1}.[23−25]

Besides a reduction in the intensity of the bands in the 900−1400 cm^{-1} range attributable to the C−O stretching vibration, upon charge the surface chemistry of the electrodes is apparently constant up to 4.4 V. Between 4.4 and 4.6 V, a massive decrease of the signals of all organic and inorganic carbonates as well as organic esters occurs. Apparently, after charge at 4.6 V, the electrodes are very similar to the pristine cathode besides a few small broad bands in the C=O and C−

O stretching range. This last evidence is in agreement with the expected occurrence of massive CO_2 release upon oxidation at voltage above 4.0−4.4 V[14] and the morphological alterations observed by TEM upon the first complete galvanostatic cycle (see previous section). Moreover, the residual presence of bands due to carbonate-based species at the end of charge suggests an incomplete electrochemical/chemical reactivity upon charge/discharge cycling.

X-ray Photoemission Spectroscopy − General. XP spectra have been recorded in different points of the first discharge−charge cycle of the cell, as reported in Figure 1 and summarized in Table 1. The binding energies (BE) corresponding to all of the species identified and analyzed in the various XP spectra are summarized in Table 2.

Table 2. Binding Energy Positions (BE) and Full Widths at Half Maximum (fwhm) Values of the Features Resulting after Theoretical Reconstruction of the Experimental XP Spectra of the Cathodes Analyzed in This Work[a]

peak	BE (eV)/fwhm (eV)	assignments
C 1s	284.3/1.1	graphitic-like (carbon support)
	285.3/1.3	C defects
	286.7/1.4	epoxy, C=O (oxidized graphite)
	287.3/1.5	C−O (TEGDME)
	289.3/5.0	graphite shakeup
	288.9−289.5/1.4	−COO−, −COOH
	289.9−290.5/1.4	−O(C=O)O− carbonate
	292.1−292.6/1.1	−CF_2− in binder
	293.3/1.4	−CF_3 in $CF_3SO_3^-$
Li 1s	55.4/1.2	Li_2O
	56.2/1.2	Li_2O_2
	56.8/2.0	Li in $LiCF_3SO_3$
S 2p	168.6−169.4/1.3	S in $LiCF_3SO_3$
F 1s	689.5/1.7	−CF_2− in binder
	689.9/1.7	−CF_3 in $CF_3SO_3^-$
	685.7/1.6	F^-

[a]Associated assignments are also reported.

X-ray Photoemission Spectroscopy − Li 1s. The Li 1s region in the XP spectrum is shown in Figure 5 for all of the studied cathodes, with the exception of the pristine clean carbon cathode, which do not contain any Li compound.

The reference signal of the Li^+ ion in the triflate salt is shown in spectrum a, at 56.8 eV, in the BE range typical of a Li salt.[26] In the following spectra b and c, the XPS features due to the typical lithiated reaction products accumulated on the carbon cathode upon discharge to 2.5 and 2.0 V can be observed. The XPS fingerprints of Li_2O and Li_2O_2 are expected to appear in the range between 54 and 56 eV, but with a roughly constant energy separation of 1 eV.[27−31] These signals are considerably down-shifted in the BE scale as compared to the pristine triflate salt value, as a result of a diminished electropositive polarization in Li when involved in a more covalent bond. Lithium peroxide, according to a simple chemical shift argument, based on the relative atomic concentration of Li and O in its formula, is reasonably expected to display a higher Li 1s BE than Li_2O.[27−31] In the hereinafter described Li 1s spectra, the two components deriving from the best fit of the experimental signal have been attributed solely to Li_2O_2 and Li_2O, on the basis of the FTIR results on the same samples and coherently with reference data reported in the literature.[30,31]
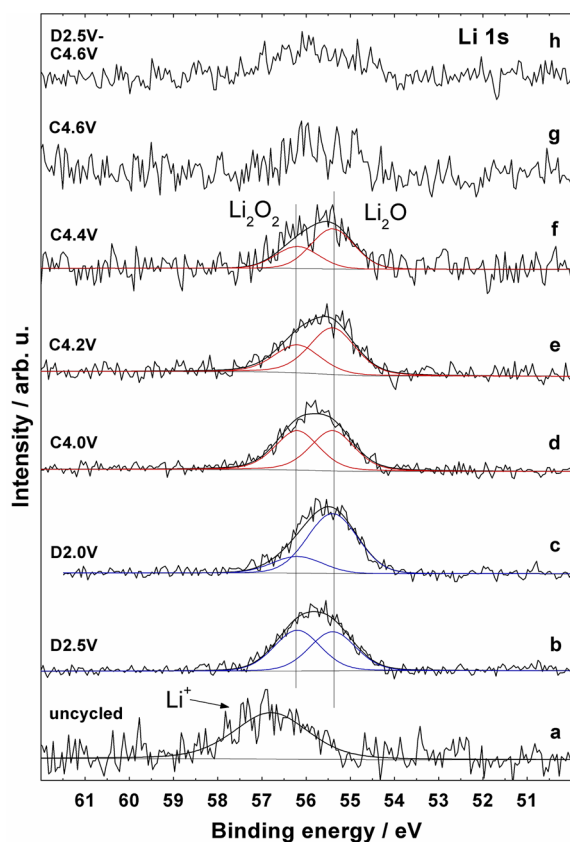
Figure 5. Li 1s XP spectra of uncycled (black line, spectrum a), discharged (blue lines, spectra b and c), and cycled (red lines, spectra d−h) carbon cathodes of the TEGDME/LiTfO Li−O_2 cell addressed in this work. Fitting results are reported as continuous lines (−).

The spectrum of the D2.5V sample shows a broad Li 1s signal, which needs both oxide (55.4 eV) and peroxide (56.2 eV) components for its reconstruction, in a near 1:1 area ratio. On the other hand, in the spectrum of the D2.0V sample, the lithium discharge compounds are mainly in the oxide form, with only a small fraction of peroxide. According to the reaction mechanism proposed in the literature,[12] lithium peroxide generates from O_2 reduction (involving the highly reactive superoxide anion) and evolves to lithium oxide already at 2.5 V. The latter becomes the main product for deeper discharges down to 2.0 V. Apparently, in both D2.5V and D2.0V samples, no other signals can be observed nor related to residual physisorbed triflate salt molecules, either from other typical chemical species like lithium carbonate or lithium fluoride, possibly formed as reaction byproducts.[14]

In Figure 5d−g are shown the Li 1s spectra recorded for the charged samples. Apparently, the S/N ratio decreases for samples charged from 4.0 to 4.6 V, although all spectra have been acquired keeping constant the recording conditions (e.g., number of scans, sample position, X-ray anode power). This evidence highlights the expected decomposition of the lithium peroxide and oxide upon charge. Going more into detail, although the experimental signals are rather weak, an attempt to reconstruct them by a two-components fitting has been performed to draw some trends. In spectrum d (sample C4.0V), peroxide and oxide components have roughly a 1:1 ratio, whereas in spectrum e (sample C4.2V), the peroxide peak decreases and so further in spectrum f (sample C4.4V). Spectra g and h show the Li 1s region of the two carbon cathodes

discharged to 2.0 and 2.5 V, and both recharged to 4.6 V, samples C4.6V and D2.5V−C4.6V, respectively. The observed signal is very small and rather noisy, thus making arbitrary any possible fitting. It is likely that after charge to potentials as high as 4.6 V, the amount of lithiated compounds at the cathode is dramatically reduced, yet with possible residues of lithium oxide.[32]

In summary, upon charge to 4.0 V, most of the Li_2O is apparently oxidized back to Li_2O_2, whereas the latter fades and almost disappears for higher anodic cutoff potentials.

Also, for charged samples no signals of other lithiated phases have been observed in the Li 1s range, like Li_2CO_3 or LiF, although the FTIR spectra highlight the formation of the inorganic lithium carbonate as reaction byproduct at the end of discharge.

Before continuing, some additional comments are required to fully discuss the lack of XPS fingerprints of Li_2CO_3 in the Li 1s spectra, in contradiction with our FTIR data and the available literature.[14] First, it is worth mentioning that in the literature, dramatically different Li 1s ionization energies in Li_2CO_3 have been reported,[19,26,28,29,33,34] ranging between 54.6 and 57.8 eV. Apparently, in our Li 1s spectra, at these BE values, no signal can be detected in our spectra, although the entire mentioned range partially overlaps with the oxide/peroxide lines. On the other hand, the absence of a signal easily attributable to Li_2CO_3 in our Li 1s XP spectra can be explained by considering (a) the intrinsically low photoionization cross-section of the Li 1s orbital[13] and (b) the possible photoelectron attenuation due to the formation of the inorganic carbonates at the buried interface between Li_2O_2 particles and the carbon support. This second hypothesis is in agreement with the findings of McCloskey et al.[35] In fact, they suggest that the inorganic carbonate is formed as a thin compact layer between the carbon electrode and the Li_2O_2 product particles. Its formation is driven by the high thermodynamic driving force for the chemical reaction of Li_2O_2 with C and also by decomposition of the electrolyte, most likely by electrochemistry at the Li_2O_2−electrolyte interface.

Turning to LiF, it has recently been reported to be the result of the degradation of Kynar, a fluorinated copolymer commonly used as binder in carbon cathodes, which is likely to undergo degradation in the presence of Li_2O_2 and either a carbonate or an ether-based solvent.[36] In our study, the lack of spectral features at 56−57 eV in the Li 1s region may suggest the absence of LiF in the outer layer of the precipitates on the surface of the cathode.[37,38]

X-ray Photoemission Spectroscopy − C 1s. Figure 6 shows C 1s spectra of the carbon cathodes. Figure 6a and b shows the pristine clean cathode before and after wetting in the electrolyte solution (1 m TEGDME/LiTfO), before any operation in the cell. These preliminary measurements have been recorded as benchmarks to make easier the interpretation of the complex envelope of peaks in the different steps of the cell lifecycle.

Figure 6c−i shows the C 1s regions of the cathode discharged to 2.5 and 2.0 V (samples D2.5V and D2.0V, respectively) and recharged to 4.0, 4.2, 4.4, and 4.6 V (samples C4.0V, C4.2V, C4.4V, and C4.6V), as well as the spectrum of the cathode from the cell discharged to 2.5 V and recharged to 4.6 V (sample D2.5V−C4.6V).

The C 1s spectrum of the reference carbon support (Figure 6a) displays the typical contributions from a lowly ordered graphitic carbon material. It shows a predominant sp^2-
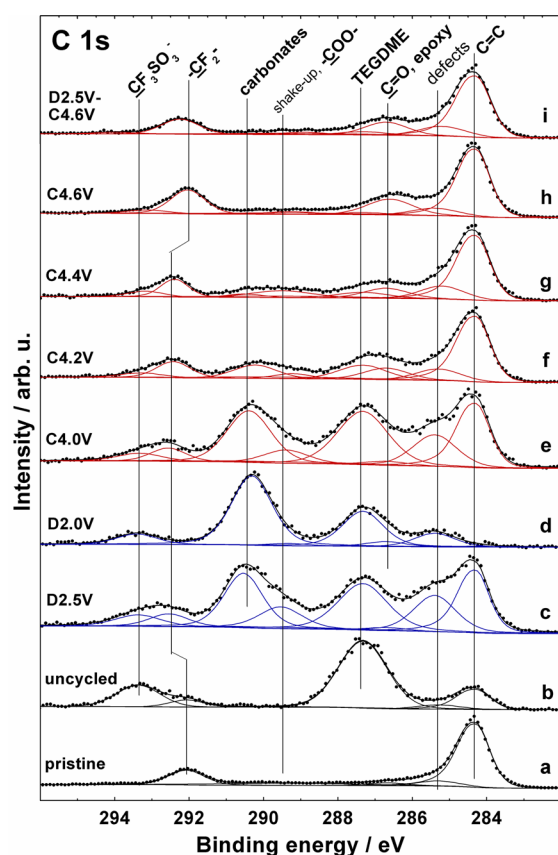
Figure 6. C 1s XP spectra of pristine and uncycled (black lines, spectra a and b), discharged (blue lines, spectra c and d), and cycled (red lines, spectra e–i) carbon cathodes of the TEGDME/LiTfO Li–O$_2$ cell addressed in this work. Fitting results are reported as continuous lines (–).

hybridized C signal at 284.3 eV, slightly asymmetric at its high BE side,[39,40] followed by a peak at 285.3 eV attributable to defects, such as sp^3-hybridized C sites, typical of high surface area graphitic materials,[41] and traces of oxidized graphite that show up at 286.7 eV, a BE value compatible with C=O and epoxy groups in graphitic materials.[41,42]

A further component, typical of extended π-delocalized carbonaceous systems, is the broad shakeup transition at 289.3 eV,[39–41] which roughly accounts for 10% of the main feature intensity. At 292.1 eV, a component due to the fluorinated binder of the cathode can be found, associated with –CF$_2$– groups.

The same C components can be detected also in Figure 6b ("uncycled") with more intense additional features at 287.3 and 293.4 eV, associated with the ethereal C–O bond in physisorbed TEGDME[26] and with CF$_3$SO$_3^-$ anion,[26,43] respectively.

Figure 6c shows the effects of discharging the cell to 2.5 V. Signals similar to those in the reference spectra (a and b) can be identified, although with different relative intensities. The signals associated with the electrolyte (287.3 and 293.4 eV) are present with a smaller intensity relative to the graphite-like carbon signal (284.3 eV). The defects-related feature at 285.3 eV is significantly enhanced, whereas the C=O/epoxy contribution at 286.7 eV remains nearly undetectable. The former component, as will be clearer in the following description, is particularly intense in the discharged samples, whereas it is found to decrease upon recharging. It is likely due

to defective graphitic surfaces originated after a nucleophilic attack of the SuperP particles from the reactive oxygen species (radicals and ions) formed by reduction of the O$_2$ gas at the cathode.

As compared to the reference spectra above-described, two additional features appear in the C 1s spectrum of the D2.5V sample: one at 289.5 eV and another at 290.1 eV both attributable to oxidized carbon atoms. The first signal can be assigned to carbon atoms in carboxylate and ester groups. These species might represent both an intermediate step of oxidation of the carbon support and a degradation product of TEGDME, as shown by Edström et al. by directly exposing it to Li$_2$O$_2$ particles.[36] The second new spectral feature at 290.1 eV can be attributed to C atoms in carbonate groups.[26,37]

When the cell is discharged down to 2.0 V, that is, for the D2.0V sample, the C 1s spectrum (Figure 6d) shows that the carbon support signals (at 284.3 and 292.1 eV) nearly disappear, while the defect features are enhanced. The depression of the intensity of the graphite-like C signal could be related to photoelectron attenuation due to deposition of lithiated products over the surface of the SuperP particles surface. The electrolyte features (287.3 and 293.4 eV) are both visible and quite intense, while the carbonate peak (290.1 eV) dominates the whole envelope of signals. On the other hand, the carboxylate peak (~289.5 eV) has almost disappeared, suggesting that these species have been completely oxidized to carbonates in deeply discharged samples.

Overall, far from being an electrochemically inert material, the amorphous carbon of the electrode results to be remarkably impacted by the reactions occurring at the interphase during discharging, and is therefore supposed to contribute to the global performance of the cell. On the other hand, as compared to the D2.5V sample, the D2.0V cathode shows a rather damaged surface, possibly covered by a thick layer of deposited material. Therefore, a more conservative anodic cutoff potential (above 2.0 V) preserves the carbon surface from massive deterioration.

The appearance of oxidized carbon species at the surface of carbonaceous cathodes after cell discharge has already been reported, especially in the presence of carbonate-based electrolytes.[14,36,37,44–48] In our case, where the ether TEGDME solvent is used, organic carbonate molecules are absent, and, therefore, upon reduction, the formation of carbonate by-products on the cathode of a Li–O$_2$ cell can only be ascribed to a purely chemical reaction mechanism involving freshly generated oxygen reduction products, such as the highly reactive superoxide and peroxide anions (O$_2^-$ and O$_2^{2-}$), and Li$_2$O$_2$.

These undesired reactions imply an irreversible consumption of O$_2$ during cell operation, which may constitute a relevant cause of the efficiency loss of the battery.

Besides organic carbonates, also inorganic Li$_2$CO$_3$ can precipitate as byproduct of parasitic reactions in many ether-based electrolytes,[14] although use of the particularly stable TEGDME/LiTfO couple has been reported to prevent its formation.[49,50] In our case, the Li$_2$CO$_3$ fingerprint is missing in the Li 1s spectra, but has been detected by FTIR spectroscopy in samples discharged down to 2.0 V. Its presence is always accompanied by other vibrational features attributable to organic carbonates (as, for example, –O(CO)O– moieties bound to the graphitic domains of the carbon electrode). Although TEGDME has been reported to limit its oxidization to carboxylate species when exposed to Li$_2$O$_2$,[36,51] we believe

the component at 290.1 eV in the C 1s XP spectra may have a 2-fold origin, both inorganic (Li_2CO_3) and organic (TEGDME solvent degradation and carbon cathode oxidation).

C 1s spectra from Figure 6e−h are associated with cells discharged to 2.0 V and recharged to 4.0, 4.2, 4.4, and 4.6 V, respectively. Overall, they display the same sequence of signals of the previously described spectra, but with variations in the relative intensities that lead at the end of charge to a spectrum similar to that of the pristine "clean" carbon cathode.

A closer look at the variations encountered by each of the peaks on going from Figure 6e−h points out the following: (i) the graphitic-like peak is more clearly visible, as its intensity becomes predominant over the other features; (ii) the defects-related signal is increasingly depressed, as are all of the highly oxidized carbon features. Interestingly, the carbonates peak, which is still intense when charging stops at 4.0 V, appears significantly reduced in the cathodes charged to 4.2 V and higher potentials. Such a decrease of the carbonates signal is in perfect agreement with the FTIR results (Figure 4) and confirms indirectly the expected further oxidation of the reaction byproducts to CO_2.[14,35]

When the cell is stopped at 4.4 and 4.6 V, residual intensities are observed in the region of C=O/epoxy and carboxylate groups. The intensity of the former component increases in parallel with the anodic cutoff potential, which suggests that the formation of the related species may be electrochemically driven. As to the TEGDME peak, its intensity interestingly decreases as the charging potential increases, and appears to be closely associated with the presence of $CF_3SO_3^-$ anion and carbonate peaks.

While the graphitic-like peak grows in intensity along with the increase of the charge end potential, so does the −CF_2− signal, this being characteristic of the bare cathode as well. As compared to the spectra of the pristine and the uncycled cathodes (Figure 6a and b, respectively), the −CF_2− signal in Figure 6c−g (samples discharged and partially charged) displays a systematically positive BE shift (+0.4−0.5 eV), possibly due to a limited reactivity of the polymeric texture during cell operation. Such an energy shift is apparently reversible and almost completely recovered in Figure 6h and i, at the end of the charge. Commercially available fluorinated binders, such as Kynar, in carbon cathodes for Li−O_2 batteries have been reported to be partially reactive when exposed to ethereal solutions in the presence of Li_2O_2,[36,51] with fluoride-based species formed as possible degradation byproducts. In our case, fluoride species were indeed detected in the F 1s region (see next section), although, at present, the behavior of the −CF_2− component in the C 1s spectrum remains unexplained.

Turning to the D2.5V−C4.6V sample, the corresponding C 1s spectrum is reported in Figure 6i. In this case, similar to the sample C4.6V, the C 1s envelope of peaks is very similar to that of pristine clean carbon support, thus highlighting an almost complete disappearance of carbonates/carboxylates and solvated anion features in comparison to the D2.5V sample. Apparently, only a residual intensity associated with C=O/epoxy groups on the carbon support can be detected at the end of charge. The spectral similarity with the uncycled carbon support, together with the high reversibility displayed in the first galvanostatic cycle (see Table 1), suggests that cycling in the 2.5−4.6 V potential range limits the electrochemical and chemical formation of byproducts on the cathode surface upon discharge and enhances their oxidation upon charge.

X-ray Photoemission Spectroscopy − Other Core Level Signals.
S 2p spectra are reported for all of the samples in Figure S2. Even if the samples were thoroughly washed with TEGDME/THF after operation in the cell, the S 2p feature attributable to triflate salt is clearly identified in all samples. The BE position of its 3/2 spin−orbit component ranges between 168.6 and 169.9 eV, with no clear trend. This range is typical for triflate anion,[52,53] whose reference spectrum is reported in Figure S2a.

Figure S3 reports the F 1s XP region for all of the investigated samples. One predominant component is discernible, located at 689.45 eV in spectra a, h, and i. It is easily assigned to the fluorinated backbone of the cathode binder, mainly composed of −CF_2− groups.[19,26,51] Besides the pristine materials, this component is dominant in the C4.6V and D2.5 V−C4.6V samples (spectra h and i). In spectra b−g of Figure S3, the most intense signal is at 689.9 eV and is easily assigned to the fluorine atoms in the triflate anion. This trend is in agreement with the C 1s spectra, where the salt component around 293 eV is evident in the same sequence of spectra (b−g).

In Figure S3c−g, a further contribution arises at 685.7 eV, possibly associated with an inorganic fluoride compound, like LiF. It is to be noted that the corresponding signal has not been observed in the Li 1s spectra. However, similar to the case of the Li_2CO_3, the lack of this signal may be related to the attenuation of the weak photoemission signal of lithium due to possible layers precipitated over the LiF particles (see above). The origin of this inorganic fluoride species is likely related to the minor degradation of the fluorinated binder, as already discussed by Edström et al.,[36,51] as the triflate anion has been reported to be one of the most stable salts used in Li−air devices.[51,52]

The O 1s XP spectra for all of the samples are reported in Figure S4. In this case, given the broadness of the featureless photoemission signals detected, no attempts have been made to deconvolute the different contributions to the signal by means of a fitting procedure. Therefore, only a qualitative description is here sketched.

The pristine cathode displays a noisy and low signal, likely attributed to oxygen atoms from the oxidized carbon support. The uncycled (Figure S4b) reference shows a positively shifted feature, which is in keeping with the presence of the TEGDME-solvated triflate anion.[53] Upon cycling (Figure S4c−i), a downshift in BE is detected for the O 1s peak. This is coherent with the formation of carbonate compounds and Li_2O_2/Li_2O species, as evidenced above by the C 1s and Li 1s spectra.[53,54] In Figure S4c−g, and especially in spectrum d, an asymmetry at the low-BE side of the O 1s peak can be seen. This shoulder is compatible with the presence of Li_2O_2/Li_2O species, formed during discharge and almost completely dissolved upon charging. Spectra h and i show a depression of this low-BE shoulder, and the photoionization peak becomes more symmetrically centered around the position of the noisy feature of spectrum a. Overall, these spectra confirm and reinforce the outcome of the more informative regions C 1s and Li 1s described above.

X-ray Photoemission Spectroscopy − Valence Region.
In Figure 7 is reported the photoionization region within the BE range of 0−22.5 eV for all of the samples. In the valence region, with X-ray exciting sources, photoionization cross sections are much lower than for excitation of electrons from the core levels, and the resulting signal intensity is poor. For
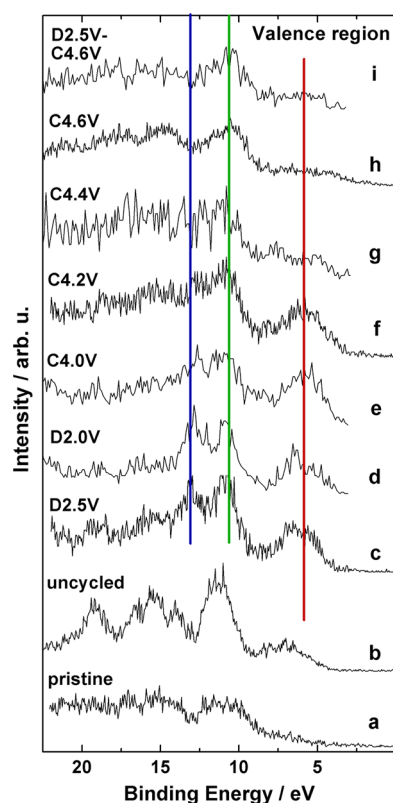
Figure 7. XP spectra of valence ionization region of pristine and uncycled (spectra a and b), discharged (spectra c and d), and cycled (spectra e–i) carbon cathodes of the TEGDME/LiTfO Li–O$_2$ cell addressed in this work. Red, green, and blue lines indicate the position of relevant features, as described in the text.

this reason, as far as we know, very limited attempts have been made so far to exploit this spectral range to investigate Li–O$_2$ cell materials. On the other hand, the kinetic energy of the emitted photoelectrons is very high, close to the energy of the used X-ray exciting photon, which results in a rather significant thickness of the sampled layer, due to a correspondingly long photoelectron inelastic mean free path. In this view, here we make a first attempt to show and comment on this region.

Starting from spectrum a in Figure 7 (pristine sample), the density-of-states (DOS) at the surface of the pristine carbonaceous cathode can be detected, mostly dominated by the lowly ordered graphitic carbon material. In this sample, as expected for graphite-like materials, DOS gradually rises only after 5 eV, whereas it is close to zero for BE < 5 eV.[55,56] In spectrum b (uncycled material), a sequence of six bands showing up roughly at 6.9, 11.3, 13.5, 15.3, 16.5, and 19.2 eV can be found, likely attributable to ionization of molecular orbitals of the TEGDME/LiTfO couple. To our knowledge, neither ionization spectra nor theoretical calculations on the valence region of LiTfO and TEGDME have been reported in the literature. However, as reported in spectra c and d, the discharge to 2.5 and 2.0 V causes a modification in the signals of the valence region. In fact, the signals of the TEGDME/LiTfO couple are somewhat depressed, and the dominant ones become those highlighted in the figure with red, green, and blue straight lines throughout the spectra. The red line indicates a contribution spanning in the range 5.4–6.4 eV, which might partially contain a signal from the TEGDME/LiTfO couple (see spectrum b) and the O 2p-dominated DOS from

Li$_2$O.[29,57,58] The other two main bands are indicated by green and blue lines, the former (around 10.7 eV) being likely attributable to O 2p-dominated DOS from Li$_2$O$_2$.[29] The contribution around 13.0 eV, indicated by a blue line, is compatible both with ionization of O 2p-like bands in lithium superoxide (LiO$_2$)[29] and with an admixture of C 2s, C 2p, and O 2p bands from carbonates.[29,59] Although the presence of superoxide-like species has been suggested in the discharge products of a TEGDME/LiTfO-based Li–O$_2$ battery,[60,61] the high reactivity of this chemical species makes unlikely its presence in our samples, which have been washed with solvents before XPS characterization. Thus, we assign the third band at 13.0 eV predominantly to carbonates. Furthermore, this component is predominant in the 2.0 V-discharged sample (spectrum d), wherein the deep discharge potential is more likely to favor transformation of the possible LiO$_2$ into lithium oxide.

The direct comparison of the variation in intensity of the band at 13.0 eV and the carbonate signals in the C 1s ionization spectra of Figure 6 (at 289.9–290.5 eV) along the differently discharged/charged samples suggests that the two signals roughly follow the same trend. In fact, carbonate deposits are mostly found in the 2.5 V- and 2.0 V-discharged cathodes and in the 2.0–4.0 V cycled cathode (spectra c–e in both Figures 7 and 6, respectively).

Similarly, the relative intensity ratio of the bands associated with Li$_2$O and Li$_2$O$_2$ (as indicated by the red and green lines in Figure 7) matches well the corresponding features in the Li 1s region (see Figure 5). The 2.5 V-discharged cathode (Figure 7c) presents both contributions from O 2p bands of the lithium peroxide and oxide, as confirmed in the corresponding Li 1s spectrum (Figure 5b). A deeper discharge, down to 2.0 V (Figure 7d), results in an intensity decrease of the Li$_2$O$_2$ feature, while upon recharge the Li$_2$O partially oxidizes to Li$_2$O$_2$ (spectra e and f). Upon increasing the charging potential (spectra g–i), the overall amount of Li compounds decreases and the valence region spectrum more closely resembles that of the pristine carbon cathode (spectrum a). This same trend is confirmed by the very low signal detected in the corresponding Li 1s region (Figure 5, spectra f–h).

The qualitatively acceptable correspondence established in these samples between the core level signals and the valence band features encourages one to explore in more depth the valence region, possibly with an ad hoc planned mixed experimental/theoretical approach. This activity is in progress in our laboratory and will be reported elsewhere on similar chemical systems.

■ CONCLUSIONS

In this work, we have investigated the evolution of the morphology and composition at the surface of a commercial Super P carbon-based cathode in the first discharge/charge cycle in a Li–O$_2$ cell with the TEGDME/LiTfO solvent/electrolyte couple. We exploited a powerful mixed analytical approach based on X-ray photoemission spectroscopy (XPS), Fourier transform infrared spectroscopy (FTIR), and transmission electron microscopy (TEM). All of the experiments were carried out ex situ on electrodes recuperated from electrochemical cells stopped at different points of their galvanostatic discharge and charge cycles: 2.5 and 2.0 V in discharge; 4.0, 4.2, 4.4, and 4.6 V in charge.

The analysis of the XP spectra, acquired in the Li 1s, C 1s, S 2p, F 1s, O 1s, and valence ionization regions, together with that of the FTIR spectra suggest the following:

(i) Oxygenated lithium compounds (Li_2O_2 and Li_2O) form upon discharge and reversibly decompose upon charge. The XPS technique was able to identify the corresponding Li peroxide and oxide contributions, sustained by FTIR, which allowed a qualitative identification/discrimination between the two phases. Li_2O_2 was found to form during discharge at 2.5 V, followed by transformation into Li_2O around 2.0 V. Upon recharge an almost complete decomposition of the Li deposits was detected, stepping through a partial oxidation of Li_2O to Li_2O_2, which eventually evolves O_2 upon further oxidation.

(ii) Carbonates/carboxylates are formed in discharge: these oxidized carbon byproducts are constituted by Li_2CO_3 and organic carbonates/carboxylates. This finding is in agreement with the model reactivity of the carbon/electrolyte/O_2 triple interphase in discharge proposed by McCloskey et al.[35] These compounds are readily dissolved upon charging up to 4.6 V, likely to CO_2.

(iii) The concentration of naturally occurring defective sites at the surface of Super P carbon is enhanced upon discharge and partially recovered during charging. This evidence suggests a direct role played by these defective carbon sites on the graphitic surfaces with the accumulation of lithiated phases (Li_2O_2, Li_2O) and the degradation byproducts. Moreover, the parallel trends detected for the intensity variation of the signals associated with the TEGDME/LiTfO couple, the carbonate compounds, and the defective graphite-like carbon, which all tend to decrease simultaneously during charging, suggest a synergistic effect where the presence of surface defects probably fosters the formation of aggregates of carbonate precipitates and solvent/salt molecules.

(iv) The formation of carbonate compounds during discharge is likely a chemically driven process, due to the spontaneous reactivity of the cell components (cathode/electrolyte) toward highly reactive species, such as superoxide anions. On the other hand, their dissolution, together with the parallel Super P oxidation, are electrochemically driven processes occurring upon charge. In fact, the characterization of the cathodes cycled to 4.6 V (samples C4.6V and D2.5V− C4.6 V) revealed that most degradation products formed during discharge are reversibly removed in charge, rendering the cathode fully available to host the reactions of the next discharge/charge cycle. Also, in this case our interpretation is in agreement with the model reactivity of the carbon/electrolyte/O_2 triple interphase in charge proposed by McCloskey et al.[35] As to the stability of the Li salt and the fluorinated binder of the cathode, the results of the present work confirm the integrity of the former and the partial reactivity of the latter.

Overall, carbonaceous cathodes used with TEGDME/LiTfO electrolyte are far from being inert catalytic supports and actively participate in the electrochemical processes occurring at their surfaces. They likely promote the formation of carbonate deposits, which contribute to the global capacity of the cell during charge. Given that at the surface of the electrode a close relationship lies between the carbonate deposits and the TEGDME/LiTfO couple, further experiments are needed to unravel the possible role of solvent/salt couple in facilitating the degradation of the carbonates during charge.

ASSOCIATED CONTENT

Supporting Information

The Supporting Information is available free of charge on the ACS Publications website at DOI: 10.1021/acsami.5b05202.

Further TEM pictures and XP spectra of the samples studied in this Article (PDF)

AUTHOR INFORMATION

Corresponding Author
*Phone: +39 0649913344. Fax: +39 06490324. E-mail: andrea.marrani@uniroma1.it.

Notes
The authors declare no competing financial interest.

REFERENCES

(1) Rui, X.; Tan, H.; Yan, Q. Nanostructured Metal Sulfides for Energy Storage. *Nanoscale* **2014**, *6*, 9889−9924.

(2) Ellis, B. L.; Knauth, P.; Djenizian, T. Three-Dimensional Self-Supported Metal Oxides for Advanced Energy Storage. *Adv. Mater.* **2014**, *26*, 3368−3397.

(3) Soloveichik, G. L. Battery Technologies for Large-Scale Stationary Energy Storage. *Annu. Rev. Chem. Biomol. Eng.* **2011**, *2*, 503−527.

(4) Tarascon, J.-M.; Armand, M. Issues and Challenges Facing Rechargeable Lithium Batteries. *Nature* **2001**, *414*, 359−367.

(5) Scrosati, B.; Garche, J. Lithium Batteries: Status, Prospects and Future. *J. Power Sources* **2010**, *195*, 2419−2430.

(6) Armand, M.; Tarascon, J.-M. Building Better Batteries. *Nature* **2008**, *451*, 652−657.

(7) Abraham, K. M.; Jiang, Z. A Polymer Electrolyte−Based Rechargeable Lithium/Oxygen Battery. *J. Electrochem. Soc.* **1996**, *143*, 1−5.

(8) Yang, Z.; Zhang, J.; Kintner-Meyer, M. C. W.; Lu, X.; Choi, D.; Lemmon, J. P.; Liu, J. Electrochemical Energy Storage for Green Grid. *Chem. Rev.* **2011**, *111*, 3577−3613.

(9) Bruce, P. G.; Freunberger, S. A.; Hardwick, L. J.; Tarascon, J.-M. Li−O_2 and Li−S Batteries with High Energy Storage. *Nat. Mater.* **2011**, *11*, 19−29.

(10) Lu, J.; Amine, K. Recent Research Progress on Non-aqueous Lithium-Air Batteries from Argonne National Laboratory. *Energies* **2013**, *6*, 6016−6044.

(11) McCloskey, B. D.; Bethune, D. S.; Shelby, R. M.; Mori, T.; Scheffler, R.; Speidel, A.; Sherwood, M.; Luntz, A. C. Limitations in Rechargeability of Li-O_2 Batteries and Possible Origins. *J. Phys. Chem. Lett.* **2012**, *3*, 3043−3047.

(12) Freunberger, S. A.; Chen, Y.; Drewett, N. E.; Hardwick, L. J.; Bardé, F.; Bruce, P. G. The Lithium−Oxygen Battery with Ether-Based Electrolytes. *Angew. Chem., Int. Ed.* **2011**, *50*, 8609−8613.

(13) Scofield, J. H. Hartree-Slater Subshell Photoionization Cross-Sections at 1254 and 1487 eV. *J. Electron Spectrosc. Relat. Phenom.* **1976**, *8*, 129−137.

(14) Imanishi, N.; Luntz, A. C.; Bruce, P. G. *The Lithium Air Battery: Fundamentals*; Springer Publishing: New York, 2014.

(15) Hummelshøj, J. S.; Luntz, A. C.; Nørskov, J. K. Theoretical Evidence for Low Kinetic Overpotentials in Li-O_2 Electrochemistry. *J. Chem. Phys.* **2013**, *138*, 034703−034712.

(16) Lu, Y.-C.; Shao-Horn, Y. Probing the Reaction Kinetics of the Charge Reactions of Nonaqueous Li−O_2 Batteries. *J. Phys. Chem. Lett.* **2013**, *4*, 93−99.

(17) Zhai, D.; Wang, H.-H.; Lau, K. C.; Gao, J.; Redfern, P. C.; Kang, F.; Li, B.; Indacochea, E.; Das, U.; Sun, H.-H.; Sun, H.-J.; Amine, K.; Curtiss, L. A. Raman Evidence for Late Stage Disproportionation in a Li−O₂ Battery. *J. Phys. Chem. Lett.* **2014**, *5*, 2705−2710.

(18) Brutti, S.; Gentili, V.; Menard, H.; Scrosati, B.; Bruce, P. G. TiO₂-(B) as Anodes for Lithium Batteries: Origin and Mitigation of the Irreversible Capacity. *Adv. Energy Mater.* **2012**, *2*, 322−327.

(19) Verma, P.; Maire, P.; Novák, P. A Review of the Features and Analyses of the Solid Electrolyte Interphase in Li-Ion Batteries. *Electrochim. Acta* **2010**, *55*, 6332−6341.

(20) Matsuta, S.; Asada, T.; Kitaura, K. Vibrational Assignments of Lithium Alkyl Carbonate and Lithium Alkoxide in the Infrared Spectra An Ab Initio MO Study. *J. Electrochem. Soc.* **2000**, *147*, 1695−1702.

(21) Brooker, M. H.; Bates, J. B. Raman and Infrared Spectral Studies of Anhydrous Li₂CO₃ and Na₂CO₃. *J. Chem. Phys.* **1971**, *54*, 4788−4796.

(22) Brooker, M. H.; Wang, J. Raman and Infrared Studies of Lithium and Cesium Carbonates. *Spectrochim. Acta, Part A* **1992**, *48*, 999−1008.

(23) Oh, S. H.; Yim, T.; Pomerantseva, E.; Nazar, L. F. Decomposition Reaction of Lithium Bis(oxalato)borate in the Rechargeable Lithium-Oxygen Cell Batteries and Energy Storage. *Electrochem. Solid-State Lett.* **2011**, *14*, A185−A188.

(24) Hase, Y.; Yoshida, I. V. P. Raman and Infrared Spectra of ⁶Li₂C₂O₄ and ⁷Li₂C₂O₄. *Monatsh. Chem.* **1980**, *111*, 1265−1272.

(25) Mouaïne, K.; Becker, P.; Carabatos-Nédelec, C. Raman and Infrared Spectra of Lithium Formate Monohydrate LiHCOO · H₂O. *Phys. Status Solidi B* **1997**, *200*, 273−287.

(26) Briggs, D.; Seah, M. P. *Practical Surface Analysis*, 2nd ed.; J. Wiley & Sons: Chichester, 1990; Vol. *1*.

(27) Yao, K. P. C.; Kwabi, D. G.; Quinlan, R. A.; Mansour, A. N.; Grimaud, A.; Lee, Y.-L.; Lu, Y.-C.; Shao-Horn, Y. Thermal Stability of Li₂O₂ and Li₂O for Li-Air Batteries: In Situ XRD and XPS Studies. *J. Electrochem. Soc.* **2013**, *160*, A824−A831.

(28) Martin, L.; Martinez, H.; Poinot, D.; Pecquenard, B.; Le Cras, F. Comprehensive X-ray Photoelectron Spectroscopy Study of the Conversion Reaction Mechanism of CuO in Lithiated Thin Film Electrodes. *J. Phys. Chem. C* **2013**, *117*, 4421−4430.

(29) Ensling, D.; Thissen, A.; Jaegermann, W. On the Formation of Lithium Oxides and Carbonates on Li Metal Electrodes in Comparison to LiCoO₂ Surface Phases Investigated by Photoelectron Spectroscopy. *Appl. Surf. Sci.* **2008**, *255*, 2517−2523.

(30) Wu, Q.; Thissen, A.; Jaegermann, W. Photoelectron Spectroscopic Study of Li Oxides on Li Over-Deposited V₂O₅ Thin Film Surfaces. *Appl. Surf. Sci.* **2005**, *250*, 57−62.

(31) Kataev, E. Y.; Itkis, D. M.; Fedorov, A. V.; Senkovsky, B. V.; Usachov, D.; Yu; Verbitskiy, N. I.; Grüneis, A.; Barinov, A.; Tsukanova, D.; Yu; Volykhov, A. A.; Mironovich, K. V.; Krivchenko, V. A.; Rybin, M. G.; Obraztsova, E. D.; Laubschat, C.; Vyalikh, D. V.; Yashina, L. V. Oxygen Reduction by Lithiated Graphene and Graphene-Based Materials. *ACS Nano* **2015**, *9*, 320−326.

(32) Because of the changes induced by the varying electrochemical conditions to the cathode surface in terms of amount and nature of the chemical species formed and deposited, an attempt to provide a semiquantitative determination of the different elements was intentionally avoided. In fact, in the absence of a "true" internal standard reference signal for XPS quantitation, the choice of a signal typical of the cathode material (e.g., F 1s) as a benchmark to which all other intensities are referred would be formally incorrect, due to the varying and uncontrolled attenuation of photoelectrons exerted by the overlying deposits in the differently obtained cathodes.

(33) Lu, Y.; Crumlin, E. J.; Carney, T. J.; Baggetto, L.; Veith, G. M.; Dudney, N. J.; Liu, Z.; Shao-Horn, Y. Influence of Hydrocarbon and CO₂ on the Reversibility of Li−O₂ Chemistry Using In Situ Ambient Pressure X-ray Photoelectron Spectroscopy. *J. Phys. Chem. C* **2013**, *117*, 25948−25954.

(34) Zhang, Z. C.; Lu, J.; Assary, R. S.; Du, P.; Wang, H. H.; Sun, Y. K.; Qin, Y.; Lau, K. C.; Greeley, J.; Redfern, P. C.; Iddir, H.; Curtiss, L. A.; Amine, K. Increased Stability Toward Oxygen Reduction Products for Lithium-Air Batteries with Oligoether-Functionalized Silane Electrolytes. *J. Phys. Chem. C* **2011**, *115*, 25535−25542.

(35) McCloskey, B. D.; Speidel, A.; Scheffler, R.; Miller, D. C.; Viswanathan, V.; Hummelshøj, J. S.; Nørskov, J. K.; Luntz, A. C. Twin Problems of Interfacial Carbonate Formation in Nonaqueous Li−O₂ Batteries. *J. Phys. Chem. Lett.* **2012**, *3*, 997−1001.

(36) Younesi, R.; Hahlin, M.; Björefors, F.; Johansson, P.; Edström, K. Li−O₂ Battery Degradation by Lithium Peroxide (Li₂O₂): A Model Study. *Chem. Mater.* **2013**, *25*, 77−84.

(37) Younesi, R.; Urbonaite, S.; Edström, K.; Hahlin, M. The Cathode Surface Composition of a Cycled Li−O₂ Battery: A Photoelectron Spectroscopy Study. *J. Phys. Chem. C* **2012**, *116*, 20673−20680.

(38) Ensling, D.; Stjerndahl, M.; Nytén, A.; Gustafsson, T.; Thomas, J. O. A Comparative XPS Surface Study of Li₂FeSiO₄/C Cycled with LiTFSI and LiPF₆-Based Electrolytes. *J. Mater. Chem.* **2009**, *19*, 82−88.

(39) Speranza, G.; Minati, L. The Surface and Bulk Core Lines in Crystalline and Disordered Polycrystalline Graphite. *Surf. Sci.* **2006**, *600*, 4438−4444.

(40) Hunt, M. R. C. Surface and Bulk Components in Angle-Resolved Core-Level Photoemission Spectroscopy of Graphite. *Phys. Rev. B: Condens. Matter Mater. Phys.* **2008**, *78*, 153408.

(41) Estrade-Szwarckopf, H. XPS Photoemission in Carbonaceous Materials: A "Defect" Peak Beside the Graphitic Asymmetric Peak. *Carbon* **2004**, *42*, 1713−1721.

(42) Barinov, A.; Malcioğlu, O. B.; Fabris, S.; Sun, T.; Gregoratti, L.; Dalmiglio, M.; Kiskinova, M. Initial Stages of Oxidation on Graphitic Surfaces: Photoemission Study and Density Functional Theory Calculations. *J. Phys. Chem. C* **2009**, *113*, 9009−9013.

(43) Blundell, R. K.; License, P. Quaternary Ammonium and Phosphonium based Ionic Liquids: A Comparison of Common Anions. *Phys. Chem. Chem. Phys.* **2014**, *16*, 15278−15288.

(44) Mizuno, F.; Nakanishi, S.; Kotani, Y.; Yokoishi, S.; Iba, H. Rechargeable Li-Air Batteries with Carbonate-Based Liquid Electrolytes. *Electrochemistry* **2010**, *78*, 403−405.

(45) Freunberger, S. A.; Chen, Y.; Peng, Z.; Griffin, J. M.; Hardwick, L. J.; Barde, F.; Novak, P.; Bruce, P. G. Reactions in the Rechargeable Lithium−O₂ Battery with Alkyl Carbonate Electrolytes. *J. Am. Chem. Soc.* **2011**, *133*, 8040−8047.

(46) Xiao, J.; Hu, J.; Wang, D.; Hu, D.; Xu, W.; Graff, G. L.; Nie, Z.; Liu, J.; Zhang, J.-G. Investigation of the Rechargeability of Li−O₂ Batteries in Non-Aqueous Electrolyte. *J. Power Sources* **2011**, *196*, 5674−5678.

(47) Xu, W.; Viswanathan, V. V.; Wang, D.; Towne, S. A.; Xiao, J.; Nie, Z.; Hu, D.; Zhang, J.-G. Investigation on the Charging Process of Li₂O₂-Based Air Electrodes in Li−O₂ Batteries with Organic Carbonate Electrolytes. *J. Power Sources* **2011**, *196*, 3894−3899.

(48) Xu, W.; Xu, K.; Viswanathan, V. V.; Towne, S. A.; Hardy, J. S.; Xiao, J.; Nie, Z.; Hu, D.; Wang, D.; Zhang, J.-G. Reaction Mechanisms for the Limited Reversibility of Li−O₂ Chemistry in Organic Carbonate Electrolytes. *J. Power Sources* **2011**, *196*, 9631−9639.

(49) Jung, H.; Kim, H.; Park, J.; Oh, I.; Hassoun, J.; Yoon, C. S.; Scrosati, B.; Sun, Y. A Transmission Electron Microscopy Study of the Electrochemical Process of Lithium−Oxygen Cells. *Nano Lett.* **2012**, *12*, 4333−4335.

(50) Jung, H.; Hassoun, J.; Park, J.; Sun, Y.; Scrosati, B. An Improved High-Performance Lithium−Air Battery. *Nat. Chem.* **2012**, *4*, 579−585.

(51) Younesi, R.; Hahlin, M.; Treskow, M.; Scheers, J.; Johansson, P.; Edström, K. Ether Based Electrolyte, LiB(CN)₄ Salt and Binder Degradation in the Li−O₂ Battery Studied by Hard X-ray Photoelectron Spectroscopy (HAXPES). *J. Phys. Chem. C* **2012**, *116*, 18597−18604.

(52) Du, P.; Lu, J.; Lau, K. C.; Luo, X.; Bareño, J.; Zhang, X.; Ren, Y.; Zhang, Z.; Curtiss, L. A.; Sun, Y.-K.; Amine, K. Compatibility of Lithium Salts with Solvent of the Non-Aqueous Electrolyte in Li−O₂ Batteries. *Phys. Chem. Chem. Phys.* **2013**, *15*, 5572−5581.

(53) Nasybulin, E.; Xu, W.; Engelhard, M. H.; Nie, Z.; Burton, S. D.; Cosimbescu, L.; Gross, M. E.; Zhang, J.-G. Effects of Electrolyte Salts on the Performance of Li−O$_2$ Batteries. *J. Phys. Chem. C* **2013**, *117*, 2635−2645.

(54) Kozen, A. C.; Pearse, A. J.; Lin, C.-F.; Schroeder, M. A.; Noked, M.; Lee, S. B.; Rubloff, G. W. Atomic Layer Deposition and in Situ Characterization of Ultraclean Lithium Oxide and Lithium Hydroxide. *J. Phys. Chem. C* **2014**, *118*, 27749−27753.

(55) Williams, P. M. The Direct Evaluation of Electronic Band Structures of Layered Solids Using Angle-Resolved Photoemission. *Nuovo Cimento B* **1977**, *38*, 216−225.

(56) Law, A. R.; Barry, J.; Hughes, H. P. Angle-Resolved Photoemission and Secondary Electron Emission From Single-Crystal Graphite. *Phys. Rev. B: Condens. Matter Mater. Phys.* **1983**, *28*, 5332−5335.

(57) Liu, L. Z.; Henrich, V. E.; Ellis, W. P.; Shindo, I. Bulk and Surface Electronic Structure of Li$_2$O. *Phys. Rev. B: Condens. Matter Mater. Phys.* **1996**, *54*, 2236−2239.

(58) Qiu, S. L.; Lin, C. L.; Chen, J.; Strongin, M. Photoemission Studies of the Interaction of Li and Solid Molecular Oxygen. *Phys. Rev. B: Condens. Matter Mater. Phys.* **1989**, *39*, 6194−6197.

(59) Thomas, S.; Sherwood, P. M. A. Valence Band X-ray Photoelectron Spectroscopic Studies of Carbonate, Bicarbonate and Formate Interpreted by Xα Calculations. *Surf. Interface Anal.* **1993**, *20*, 595−599.

(60) Zhai, D.; Wang, H.; Yang, J.; Lau, K. C.; Li, K.; Amine, K.; Curtiss, L. A. Disproportionation in Li−O$_2$ Batteries Based on a Large Surface Area Carbon Cathode. *J. Am. Chem. Soc.* **2013**, *135*, 15364−15372.

(61) Yang, J.; Zhai, D.; Wang, H.; Lau, K. C.; Schlueter, J. A.; Du, P.; Myers, D. J.; Sun, Y.; Curtiss, L. A.; Amine, K. Evidence for Lithium Superoxide-Like Species in the Discharge Product of a Li−O$_2$ Battery. *Phys. Chem. Chem. Phys.* **2013**, *15*, 3764−3771.